Published in final edited form as:
Calcif Tissue Int. 2019 January ; 104(1): 79–91. doi:10.1007/s00223-018-0471-8.

Longitudinal Examination of Bone Loss in Male Rats After Moderate–Severe Contusion Spinal Cord Injury

Dana M. Otzel[1], **Christine F. Conover**[2], **Fan Ye**[2], **Ean G. Phillips**[2], **Taylor Bassett**[2], **Russell D. Wnek**[2], **Micah Flores**[2], **Andrea Catter**[2], **Payal Ghosh**[2], **Alexander Balaez**[2], **Jason Petusevsky**[2], **Cong Chen**[3], **Yongxin Gao**[4], **Yi Zhang**[1], **Jessica M. Jiron**[5], **Prodip K. Bose**[1,5,6], **Stephen E. Borst**[7], **Thomas J. Wronski**[5], **J. Ignacio Aguirre**[5], **Joshua F. Yarrow**[2,8]

[1]Brain Rehabilitation Research Center, Malcom Randall Department of Veterans Affairs Medical Center, North Florida/South Georgia Veterans Health System, 1601 SW Archer Road, Research 151, Gainesville, FL 32608, USA

[2]Research Service, Malcom Randall Department of Veterans Affairs Medical Center, North Florida/South Georgia Veterans Health System, 1601 SW Archer Road, Research 151, Gainesville, FL 32608, USA

[3]Department of Orthopedics and Rehabilitation, University of Florida, PO Box 112727, Gainesville, FL 32611, USA

[4]University of Florida College of Medicine, Jacksonville, FL 32209, USA

[5]Department of Physiological Sciences, University of Florida, PO Box 100144, Gainesville, FL 32610, USA

[6]Department of Neurology, University of Florida, HSC PO Box 100236, Gainesville, FL 32610, USA

[7]Department of Applied Physiology and Kinesiology, University of Florida, PO Box 118205, Gainesville, FL 32611, USA

[8]Division of Endocrinology, Diabetes, and Metabolism, University of Florida College of Medicine, 1600 SW Archer Road, Gainesville, FL 32610, USA

Abstract

To elucidate mechanisms of bone loss after spinal cord injury (SCI), we evaluated the time-course of cancellous and cortical bone microarchitectural deterioration via microcomputed tomography, measured histomorphometric and circulating bone turnover indices, and characterized the

✉Joshua F. Yarrow, Joshua.yarrow@medicine.ufl.edu.

Electronic supplementary material The online version of this article (https://doi.org/10.1007/s00223-018-0471-8) contains supplementary material, which is available to authorized users.

Conflict of interest Dana M. Otzel, Christine F. Conover, Fan Ye, Ean G. Phillips, Taylor Bassett, Russell D. Wnek, Micah Flores, Andrea Catter, Payal Ghosh, Alexander Balaez, Jason Petusevsky, Cong Chen, Yongxin Gao, Yi Zhang, Jessica M. Jiron, Prodip K. Bose, Stephen E. Borst, Thomas J. Wronski, J. Ignacio Aguirre and Joshua F. Yarrow declares that they have no conflict of interest.

Human and Animal Rights and Informed Consent All experimental procedures conformed to the ILAR Guide to the Care and Use of Experimental Animals and were approved by the Institutional Animal Care and Use Committee at the Malcom Randall VA Medical Center.

development of whole bone mechanical deficits in a clinically relevant experimental SCI model. 16-weeks-old male Sprague–Dawley rats received T_9 laminectomy (SHAM, $n = 50$) or moderate–severe contusion SCI ($n = 52$). Outcomes were assessed at 2-weeks, 1-month, 2-months, and 3-months post-surgery. SCI produced immediate sublesional paralysis and persistent hindlimb locomotor impairment. Higher circulating tartrate-resistant acid phosphatase 5b (bone resorption marker) and lower osteoblast bone surface and histomorphometric cancellous bone formation indices were present in SCI animals at 2-weeks post-surgery, suggesting uncoupled cancellous bone turnover. Distal femoral and proximal tibial cancellous bone volume, trabecular thickness, and trabecular number were markedly lower after SCI, with the residual cancellous network exhibiting less trabecular connectivity. Periosteal bone formation indices were lower at 2-weeks and 1-month post-SCI, preceding femoral cortical bone loss and the development of bone mechanical deficits at the distal femur and femoral diaphysis. SCI animals also exhibited lower serum testosterone than SHAM, until 2-months post-surgery, and lower serum leptin throughout. Our moderate–severe contusion SCI model displayed rapid cancellous bone deterioration and more gradual cortical bone loss and development of whole bone mechanical deficits, which likely resulted from a temporal uncoupling of bone turnover, similar to the sequalae observed in the motor-complete SCI population. Low testosterone and/or leptin may contribute to the molecular mechanisms underlying bone deterioration after SCI.

Keywords

Osteoporosis; Bone mineral density; Disuse; Testosterone; Leptin; Sclerostin

Introduction

Sublesional osteoporosis is a hallmark of functionally complete spinal cord injury (SCI) that is precipitated both by the neurologic insult and disuse [1]. Individuals with SCI experience biphasic bone loss characterized by 50–70% lower cancellous bone mineral density (BMD) within several years of injury [2] and a more gradual 25–35% cortical bone loss over the following decade, with bone loss plateauing thereafter, despite continual paralysis [3, 4]. This severe skeletal decline results in > 20-fold higher bone fracture risk [5], with a disproportionate ratio of fractures occurring at nontraditional skeletal sites, including the distal femur and proximal tibia [6, 7].

Bone loss has been characterized in experimental rodent SCI models. Of these, the spinal cord transection model produces the most severe injury and post-injury bone loss [8]. However, spinal transection does not mimic the most prevalent injury mechanism in persons with SCI (i.e., a contusion to the spinal cord followed by brief or extended spinal compression) and eliminates descending central nervous system input to bone, suggesting pathophysiologic differences between the transection model and that observed clinically [9]. In contrast, the contusion SCI model more closely represents histopathologic features of human SCI [9]. Previous reports have delineated the acute [10–12] and more chronic skeletal adaptations in rodents after moderate–severe contusion SCI [13–15], although, study limitations persist in each. Specifically, several studies evaluated bone loss for only a few days or weeks after contusion SCI [10–12]. In addition, most SCI models have evaluated

bone loss in young (< 12-weeks-old) male [8, 10, 16, 17] or female rodents [13, 15, 18] that are undergoing bone modeling and rapid bone growth at time of injury, which is not indicative of skeletal maturity. In this regard, ~ 80% persons with SCI are males who experienced injury in adulthood [19] when bone modeling and bone growth have ceased. Recently, Lin et al. examined longitudinal skeletal changes between a small cohort of 4-month-old skeletally mature male rodents that received moderate contusion SCI ($n = 5$) and nonsurgical controls ($n = 5$) [14]. However, the longitudinal study design employed by Lin et al. did not allow for examination of histomorphometric changes in bone turnover that mediate the skeletal decline after SCI or the time course in which bone mechanical deficits develop. Indeed, we are unaware of any study that has evaluated the time course of cancellous and cortical bone loss in skeletally mature male rodents following moderate–severe contusion SCI, in relation to changes in histomorphometric and circulating bone turnover markers and whole bone mechanical characteristics. Further, the relatively common use of nonsurgical control comparators by Lin et al. [14] and others [10, 12, 13, 15, 17] confounds interpretation of bone loss after experimental SCI because the invasive surgical laminectomy required to expose the spinal cord produces local/systemic inflammation that may independently influence musculoskeletal outcomes. To control for these confounders, we used 4-months-old male rodents receiving moderate–severe contusion SCI and age-matched control animals receiving spinal laminectomy. Our purposes were to (1) characterize longitudinal changes in cancellous and cortical bone microstructure, bone turnover, and bone mechanical characteristics in our SCI model; and (2) evaluate circulating concentrations of several hormones that may influence bone maintenance.

Methods

Animal Care

Barrier-raised and specific-pathogen-free 16-weeks-old male Sprague–Dawley rats were obtained from Charles River Laboratories (Wilmington, MA). Animals were individually housed in a temperature-/light-controlled room, on 12-h light:dark cycles, and were fed rodent chow (Teklad Global 18% Protein Rodent Diet, Harlan Laboratories Inc., Indianapolis, IN) and tap water ad libitum.

Experimental Design

Rats were stratified by body mass into the following groups: (1) T_9 laminectomy (SHAM, $n = 50$) or (2) laminectomy plus moderate–severe contusion SCI ($n = 52$). Tail blood was sampled before surgery and biweekly thereafter. To characterize the functional consequences of SCI, animals were assessed weekly for open-field locomotion by two blinded observers using the Basso–Beattie–Bresnhan (BBB) locomotor rating scale [20]. Declomycin and calcein (chemicals obtained from Sigma-Aldrich, St. Louis, MO unless noted) were administered (15 mg/kg, s.c.) 10 and 3 days before sacrifice, respectively, to fluorochrome label bone surfaces. Subsets of animals were sacrificed at 2-, 4-, 8-, and 12-weeks post-surgery, via isoflurane overdose and terminal exsanguination. Blood was collected via intracardiac puncture at sacrifice, with serum stored at − 80 °C. The left and right femurs and tibiae were excised. Femurs were wrapped in saline-soaked gauze and stored at − 20 °C for subsequent microcomputed tomography (μCT) and bone mechanical assessments. The

left tibiae were prepared for histomorphometry. The T_7–T_{11} section of the spinal cord, encompassing the lesion site, was excised and fixed in 10% formalin for histological analysis.

Surgery and Postoperative Care

Surgery and postoperative care were performed according to our methods [21–23]. Briefly, anesthetized animals received a T_9 laminectomy to expose the spinal cord. A contusion SCI was produced by applying 250-kilodyne force to the T_9 spinal cord segment with the Infinite Horizons (IH) Impactor (Precision Systems and Instrumentation, Lexington, KY). Animals received buprenorphine (0.05 mg/kg, s.c.) and ketoprofen (5.0 mg/kg, s.c.) for 48 h, and ampicillin for 5 days. Postoperative care included daily examination for signs of distress, weight loss, dehydration, fecal clearance, bladder dysfunction, and skin lesions. Bladders were expressed twice daily until spontaneous voiding returned. Ringer's was provided to promote rehydration. Jell-O® with added protein/fat and apples were provided to assist in bodyweight maintenance. SHAMs received T_9 laminectomy to expose the spinal cord, without contusion injury.

Animal Model Rationale

We utilized 4-months-old skeletally mature male rats because most SCI occur in adult men [19] via a contusion impact to the spinal cord. We have reported extensive cancellous bone loss in young [21] and skeletally mature male rats [23] within 21 days of moderate–severe contusion SCI. However, our previous studies did not evaluate the time course of bone loss. We are currently unaware of any study that evaluated temporal changes in cancellous/cortical bone morphology, histomorphometric and biochemical bone turnover markers, and bone mechanical characteristics in skeletally mature male rats receiving moderate–severe contusion SCI.

Spinal Cord Histology

Following fixation and dehydration, the spinal cord was embedded in paraffin and sectioned at 10-μm thickness. Hematoxylin and eosin stained sections were evaluated using a Zeiss Axio Imager Z2 light microscope (Carl Zeiss, Göttingen, Germany) to qualitatively assess injury severity [21, 23].

Bone Histomorphometry

Cancellous and cortical bone parameters were evaluated at the proximal tibial metaphysis and diaphysis via histomorphometry, respectively [24]. In brief, tibiae were fixed in 10% phosphate-buffered formalin, dehydrated in ethanol, and embedded undecalcified in methyl methacrylate. 4-μm-thick proximal tibia sections were stained with von Kossa and counterstained with tetrachrome (Polysciences Inc., Warrington, PA) to assess cancellous bone structure. 8-μm-thick sections remained unstained to measure fluoro-chrome-based bone formation indices. The proximal tibia region of interest (ROI) began 0.5 mm distal to the growth plate and excluded the primary spongiosa and cancellous bone tissue within 0.25 mm of the endocortical border. Cortical bone was assessed using 50-μm-thick sections obtained proximal to the tibia–fibular junction. The following variables were measured with

the Osteomeasure System (Osteometrics, Decatur, GA): cancellous bone volume (BV/TV), trabecular number (Tb.N), trabecular thickness (Tb. Th), trabecular separation (Tb.Sp), and diaphyseal cortical thickness (Ct.Th). Osteoblast (Ob.S/BS) and osteoclast (Oc.S/BS) surfaces were measured as percentages of total cancellous perimeter. Fluorochrome-based indices of cancellous bone formation were measured under ultraviolet illumination. Mineralizing surface, an index of active bone formation, was calculated as the percentage of cancellous (MS/BS), periosteal (Ps.MS/BS), and endocortical (Ec.MS/BS) bone surfaces with a double-fluorochrome label. Mineral apposition rate (MAR), an index of osteoblastic activity, was calculated by dividing the interlabel distance by the time interval between fluorochrome labeling. Bone formation rate (BFR/BS) was calculated by multiplying MS/BS by MAR.

μCT Analysis of Bone Morphology

Three-dimensional bone morphology was evaluated on excised femurs with a Bruker Skyscan 1172 μCT (Kontich, Belgium) [12, 21, 22]. Images were acquired at 80kVP/120 μA, 0.5 mm Al filter, 1 k resolution, 19.9 μm voxel, 0.5° rotation step, and 180° tomographic rotation. The distal femur cancellous ROI began 2.0 mm proximal to the growth plate and encompassed 3.5 mm. This ROI was then divided into three equidistant (~ 1.17 mm) sub-ROI to determine if cancellous bone preservation differed as distance from the growth plate varied. The cortical ROI at the distal femur encompassed the most proximal 2.0 mm of the cancellous ROI, to avoid residual growth plate. The femoral diaphysis ROI encompassed 2.0 mm near the mid-shaft. Cancellous outcomes included: BV/TV, Tb.N, Tb.Th and distribution, Tb.Sp and distribution, and trabecular pattern factor (Tb.Pf). Cortical outcomes included total (bone plus medullary) area (Tt.Ar, mm^2), cortical bone area (Ct. Ar, mm^2), cortical area fraction (Ct.Ar/Tt.Ar, %), and Ct.Th. Cancellous volumetric (v)BMD and cortical tissue mineral density (TMD) were calculated after calibration with hydroxyapatite phantoms.

Bone Mechanical Characteristics

Bone mechanical characteristics were assessed at the distal femur and at the contralateral femoral midshaft, a more standard skeletal site. Evaluation of the distal femur is warranted because supracondylar femoral fractures are highly prevalent after motor-complete SCI [7] and typically result in extended hospitalization [6]. Prior to testing, the femora were thawed to room temperature and remained wrapped in saline-soaked gauze except during measurements. The right distal femur underwent a modified anterior–posterior compression and bending test [12, 22]. Briefly, the femur was cut cross-sectionally near the midshaft via Dremel (Mt. Prospect, IL). The midshaft was then embedded vertically in Bondo fiberglass resin (3M, St. Paul, MN) in the center of a rectangular cuvette, with ~ 8 mm of the most distal portion of the femur extending out of the cuvette and remaining unembedded. Prior to testing, the cuvette was affixed horizontally to the servohydraulic testing machine (MTS 858 Bionix Test System, MTX, Eden Prairie, MN) with the anterior femur facing upward (Online Resource 1a). Ten cycles of sinusoidal preload (from 0 to 10 N) were applied in the vertical direction to the anterior distal femur using a flat steel fixture attached to the MTS. The compression load was applied at 1.0 mm/s until specimen failure. Maximal load, displacement at maximal load, stiffness, and energy to fracture were determined from the

load–deformation curves. A medial–lateral 3-point bending test was performed on the contralateral femoral midshaft [24, 25]. In brief, the femur was placed in the horizontal position across two support rollers with the medial femur facing upward, and the load was applied at the diaphysis with a steel rod (Online Resource 1b), using the settings listed above.

Serum Measurements

Blood was acquired prior to surgery and biweekly thereafter, as described above. Serum hormones were measured in duplicate on a single plate and are reported as change from baseline, except for testosterone which is reported as actual concentration because insufficient baseline sera was available to calculate percentage change. Procollagen type 1 N-terminal (P1NP) and osteocalcin (bone formation markers) and tartrate-resistant acid phosphatase 5b (TRAP5b, an osteoclast derived bone resorption marker) were determined by EIA with intra-assay $CVs < 7.4\%$ (IDS, Fountain Hills, AZ). Testosterone was evaluated by EIA with intra-assay $CV < 9\%$ (ALPCO, Salem, NH). Leptin was determined by ELISA with intra-assay $CV < 2.5\%$ (Millipore, MA). Sclerostin was assessed by ELISA with intra-assay $CV < 7.2\%$ (R&D Systems, Minneapolis, MN).

Statistical Analysis

Results are reported as Means ± SEM, with $p < 0.05$ defined as the threshold of significance. Mixed-model repeated measures ANOVAs were used to analyze body mass and BBB score, which were assessed at multiple timepoints in the same animal. Group and time main effects and interactions were determined with two-way [2 (Group) × 4 (Time)] ANOVAs for all skeletal outcomes assessed at a single timepoint (2 weeks, 1 month, 2 months, or 3 months), and for serum hormone concentrations. For all ANOVAs, Tukey's post hoc tests were performed for multiple comparisons among groups. In addition, four targeted independent samples *t*-tests were selected a priori to compare differences between age-matched SHAM and SCI groups at the same postsurgical timepoint because these comparisons are the most meaningful within our study design. Data were analyzed using SPSS v24.0.0 (IBM, Chicago, IL).

Results

Postsurgical Recovery and Injury Severity

Baseline body mass was similar among SHAM (532 ± 5) and SCI (536 ± 4) groups. SCI exhibited 8–11% bodyweight loss in the 2-weeks post-injury ($p < 0.01$) and gradual bodyweight gain thereafter (Online Resource 2a). In comparison, bodyweight gradually increased in SHAMs, remaining higher than baseline from weeks 3–12 and higher than SCI throughout ($p < 0.01$). The average injury force and velocity were 310 ± 7 kdyne and 122 ± 1 mm/s, respectively. Immediately post-surgery, SCI animals displayed signs consistent with severe SCI, including hindlimb paralysis, reduced appetite and thirst, and an inability to voluntarily void the bladder. At week 1, SCI animals exhibited extensive hindlimb locomotor deficits (BBB = 1.3 ± 0.1), with some spontaneous functional recovery occurring until week 7 (BBB = 5.9 ± 0.5) and plateauing thereafter (Online Resource 2b). SCI animals did not regain hindlimb weight-supported stepping or the ability to support bodyweight in

stance at any timepoint. Recovery of appetite, thirst, and bladder function accompanied the limited hindlimb recovery after SCI. Histologic examination of spinal cords revealed findings consistent with moderate–severe SCI (Online Resource 3). At the injury epicenter, mostly symmetrical white and gray matter loss was present on both sides of the cord, with a thin layer of spared white matter remaining, predominantly in the ventral half of the cord. The spared tissue exhibited significant axonal loss, although, some preservation of myelin, axons, and collagen morphology was present. Significant tissue debris and multiple cavities were evident throughout the spinal white/gray areas. Animals euthanized at timepoints nearest to SCI exhibited the most residual debris, with less debris present in 2–3-months cords. SHAMs displayed normal spinal cord histology and unimpaired hindlimb function (BBB = 21) throughout.

Tibial Histomorphometry

Group and time main effects and interactions derived from the 2 × 4 ANOVAs are reported in Online Resource 4, with the primary findings from these analyses briefly summarized throughout the following sections. Results from the targeted independent samples *t*-tests are reported in detail within each section and are included in the accompanying figures because these comparisons are the most meaningful within our study design.

Cancellous and cortical histomorphometric outcomes are reported in Figs. 1a–i and 2a–d, respectively. Group main effects indicated that SCI exhibited lower BV/TV, Tb.N, Tb.Th, and Tb.Sp ($p < 0.001$, Online Resource 4). Time main effects indicated higher Tb.Th and lower Oc.S/BS at later timepoints ($p < 0.01$). Interactions revealed that SCI exhibited lower MS/BS, MAR, and BFR/BS at 2-weeks post-surgery versus all SHAM groups and other SCI timepoints ($p < 0.05$ to $p < 0.01$), indicative of reduced cancellous bone formation early after SCI.

Targeted *t*-tests indicated that proximal tibia cancellous BV/TV was 45–60% lower in SCI versus SHAM at all timepoints ($p < 0.05$), characterized by lower Tb.Th (2 weeks: $p < 0.01$), lower Tb.N (1–3 months: $p < 0.05$), and higher Tb.Sp (1–2 months: $p < 0.05$). In addition, Ob.S/BS was 87% lower in SCI versus SHAM at 2 weeks ($p < 0.01$), which produced lower MS/BS ($p < 0.001$), MAR ($p < 0.01$), and BFR/BS ($p < 0.001$) at this timepoint. In comparison, MAR and MS/BS were higher in SCI versus SHAM at 1-month and 2-months post-surgery, respectively, and MS/BS and BFR/BS were lower in SCI versus SHAM at 3 months (all $p < 0.05$).

At the tibial diaphysis, no group main effects were observed. Time main effects indicated higher Ct.Th and lower Ps.MAR at later timepoints ($p < 0.05$ to $p < 0.01$, Online Resource 4). Interactions revealed reduced periosteal bone formation indices in SCI at 1-month post-surgery, as indicated by lower Ps.MS/BS and Ps.BFR/BS versus all SHAM timepoints and 2–3 months SCI groups ($p < 0.05$ to $p < 0.01$). Similarly, targeted *t*-tests indicated that Ps.MS/BS was 25% lower in SCI versus SHAM at 2 weeks (*trend*, $p = 0.054$) and 60% lower at 1 month ($p < 0.001$), accompanied by 55% lower Ps.BFR/BS (1 month: $p < 0.001$). No differences in Ec.MS/BS were present among groups (data not shown). Double-fluorochrome labeling was not present on enough samples to assess Ec.MAR or Ec.BFR/BS.

μCT Analysis of Cancellous Morphology

Figure 3a–f contains representative μCT cancellous bone images and outcomes from the distal femoral metaphysis ROI. Group main effects indicated that SCI exhibited lower distal femur vBMD, BV/TV, and Tb.N, along with higher Tb.Sp and Tb.Pf ($p = 0.013$ to $p < 0.001$, Online Resource 4). Similar to histomorphometry, a time main effect indicated higher Tb.Th at later timepoints ($p < 0.01$). Interactions revealed that SCI exhibited higher Tb.Pf at 2-weeks post-surgery, indicative of a less-connected trabecular network versus all SHAM groups and other SCI timepoints ($p < 0.05$ to $p < 0.01$).

Targeted *t*-tests indicated that cancellous vBMD was 30–35% lower in SCI versus SHAM at all timepoints (2 weeks: $p < 0.001$; 1–3 months $p < 0.05$) and that BV/TV was 25–50% lower in SCI animals (2 weeks: $p < 0.001$; 1–2 months: $p < 0.05$; 3 months: $p = 0.059$, *trend*). The latter effect was less distinct as distance from the growth plate increased (Online Resource 5a–d). This bone loss was characterized by 10% lower Tb.Th at 2 weeks after SCI ($p < 0.01$) and by a more pronounced 50% reduction in Tb.N occurring within the first 2 weeks ($p < 0.001$) and persisting thereafter (1–3 months: $p < 0.05$). The lower Tb.Th resulted from a higher proportion of small trabeculae (< 0.1 mm) and lower proportions of larger trabeculae (ranging from 0.1 to 0.18 mm) that is indicative of increased bone resorption (Online Resource 6a–d). In addition, SCI produced a rightward shift in Tb.Sp distribution at all timepoints (Online Resource 7a–d), particularly at values < 0.38 mm, along with higher Tb.Pf (2 weeks: $p < 0.001$; 1 month: $p < 0.05$).

μCT Analysis of Cortical Morphology

Figure 4 contains representative μCT cortical bone images and outcomes from the distal femur (Fig. 4a–f) and femoral diaphysis ROIs (Fig. 4g–l). Group main effects indicated lower Tt.Ar (distal femur only), Ct.Ar, Ct.Ar/Tt.Ar, Ct.Th, and vTMD (diaphysis only) at both skeletal sites after SCI ($p = 0.009$ to $p < 0.001$, Online Resource 4). Time main effects indicated higher values for most cortical structural variables at later timepoints ($p < 0.05$ to $p < 0.01$), suggesting progressive cortical expansion and cortical thickening. However, interactions revealed that only SHAM animals exhibited progressively higher Ct.Ar, Ct.Ar/Tt.Ar, Ct.Th, and vTMD at the femoral diaphysis ($p < 0.05$ to $p < 0.01$), indicating minimal postsurgical cortical bone accumulation at this site after SCI.

At 2-weeks post-surgery, targeted *t*-tests indicated no cortical bone differences among groups at either site. Thereafter, distal femur Ct.Ar and Ct.Th were 7% lower in SCI versus SHAM at 1 month (both $p < 0.05$) and 10–12% lower at 2 months (Ct.Ar only $p < 0.001$) and 3 months (both $p < 0.01$). SCI also exhibited 8–10% lower femoral diaphysis Ct.Ar (2 months: $p < 0.01$; 3 months: $p < 0.05$), 5–9% lower Ct.Ar/Tt.Ar (2 months: $p < 0.001$; 3 months: $p < 0.01$), 8–9% lower Ct.Th (2 months: $p < 0.01$; 3 months: $p < 0.05$), and 2–3% lower vTMD (2–3 months: $p < 0.05$) when compared with the corresponding SHAM timepoint.

Bone Mechanical Testing

Femoral mechanical characteristics are reported in Fig. 5a–d (distal femur) and Fig. 5e–h (femoral midshaft). Group main effects indicated SCI exhibited lower maximal load,

displacement at maximal load (distal femur only), and energy to fracture at both skeletal sites ($p = 0.001$ to $p < 0.001$, Online Resource 4). Time main effects indicated higher maximal load (both sites), energy to fracture (distal femur only), and stiffness (midshaft only) at later timepoints ($p < 0.05$ to $p < 0.01$). Targeted *t*-tests revealed that distal femur maximal load and displacement were lower in SCI versus SHAM at 2-weeks (maximal load: $p < 0.05$), 1-month (maximal load: $p < 0.01$; displacement: $p < 0.05$), and 3-months post-surgery (both: $p < 0.05$), producing 29–45% lower energy to fracture after SCI (2 weeks: $p < 0.05$; 1–/3 months: $p < 0.01$). In comparison, midshaft maximal load was lower in SCI versus SHAM at 2–3-months post-surgery ($p < 0.05$), producing 21–35% lower energy to fracture after SCI (2 months: *trend,* $p = 0.061$; 3 months: $p < 0.05$).

Serum Measurements

Baseline serum hormone concentrations were similar between groups (Online Resource 8). The percentage changes in serum measurements from baseline are reported in Fig. 6a–f, except for testosterone which is reported as actual concentration because insufficient baseline sera were available. Group main effects indicated lower leptin and testosterone after SCI ($p < 0.001$, Online Resource 4). Time main effects indicated higher leptin and testosterone at later timepoints ($p < 0.05$ to $p < 0.01$). Within respective groups, interactions revealed higher leptin at 2 months and 3 months (SHAM only) when compared with earlier timepoints ($p < 0.05$ to $p < 0.01$). Time main effects also indicated lower TRAP5b, P1NP, and osteocalcin at later timepoints, suggestive of lower bone turnover across the age-span ($p < 0.05$ to $p < 0.01$). Interactions revealed lower TRAP5b in both groups at 3 months when compared with several previous timepoints ($p < 0.01$). Targeted *t*-tests revealed TRAP5b change from baseline was higher in SCI versus SHAM at 2-weeks post-surgery ($p < 0.01$), with no other differences in bone turnover markers. SCI also exhibited lower leptin than SHAM at all timepoints ($p < 0.001$) and 35–50% lower testosterone versus SHAM (2 weeks: $p < 0.01$; 1 month: $p < 0.05$; 2 months: $p < 0.01$).

Discussion

Bone loss after SCI is precipitated by the neurologic insult and subsequent disuse [1]. However, SCI-induced bone loss is more rapid and severe than that occurring in response to sciatic neurectomy [16] or immobilization-induced disuse [12, 17], suggesting that factors beyond unloading contribute to the skeletal decline after SCI. Herein, we characterized the time courses of cancellous and cortical bone deficits in a clinically relevant rodent SCI model to assist in identifying the mechanism exacerbating skeletal deterioration after SCI, which is important from a clinical perspective given that fracture incidence is associated with mortality in this population [26]. Our data indicate: (1) severe cancellous bone loss at the distal femur and proximal tibia within 2 weeks of SCI and temporally delayed cortical bone deficits thereafter, similar to the biphasic bone loss occurring in the human SCI population [3, 4]; (2) increased circulating TRAP5b, lower Ob.S/BS, and lower cancellous histomorphometric bone formation indices at 2-weeks post-SCI, similar to the uncoupled bone turnover reported in humans acutely after SCI [27]; (3) lower Ps.MS/BS and Ps.BFR/BS at 2-weeks and 1-month post-surgery, indicating a periosteal bone formation defect preceded cortical bone loss; and (4) temporal and site-specific bone mechanical

deficits, with the distal femur exhibiting earlier strength deficits than the femoral diaphysis. The persistent lack of hindlimb weight-bearing and the accompanying skeletal decline that we observed, suggests that our findings are relevant to the severe motor-incomplete and/or motor-complete SCI populations that are at risk of bone fracture [6, 7], providing content validity to our preclinical model.

Within the first few years of injury, individuals with SCI exhibit 50–70% lower BMD at the distal femur and proximal tibia [2], sites that are traditionally rich in cancellous bone, and a relative plateau in cancellous bone loss thereafter [3, 4]. Similarly, our model exhibited 30–35% lower distal femur cancellous vBMD and > 50% lower distal femur and proximal tibia BV/TV within 2 weeks of SCI. These skeletal sites are particularly relevant to the SCI population, given the high prevalence of supracondylar femoral fractures after motor-complete SCI [7] and that > 80% of fractures requiring hospitalization in the chronic SCI population occur in the tibia and femur [6]. The cancellous bone deficits in our model were characterized by lower Tb.Th and Tb.N, a rightward shift in the Tb.Sp distribution, and higher Tb.Pf within 2 weeks of SCI. Moreover, SCI exhibited a larger increase in circulating TRAP5b than SHAM at 2 weeks, albeit no differences in Oc.S/BS were present among groups at any timepoint. These results suggest that existing osteoclasts exhibited increased resorptive activity, as others have reported [10, 11], which could be verified in future studies by assessing TRAP-positive osteoclasts. Despite this increased bone resorption, Ob.S/BS and all cancellous histomorphometric bone formation indices were markedly lower in SCI at 2 weeks. In comparison, sex-hormone deficiency produces concurrently increased bone resorption and formation [24], demonstrating SCI-induced bone loss is characteristically different than high-turnover osteopenia. Our findings suggest that the SCI-related uncoupling of bone turnover that has been observed in humans [27] and other experimental SCI models [10, 11] likely results from impaired bone anabolic signaling [28]. Consistent with this notion, Zhao et al. observed fewer alkaline phosphatase-positive colonies and fewer mineralized nodules in cultured bone marrow-derived stem cells extracted from spinal transected versus sham animals, indicating fewer mesenchymal progenitors were recruited into the osteoblastic lineage in response to SCI [29]. Despite this evidence, circulating osteocalcin and P1NP were similar among groups, perhaps because relatively normal bone formation exists above the spinal lesion and/or because longitudinal bone growth contributes to circulating bone formation markers until rodents are aged ~ 60 months [30, 31]. In this regard, both groups exhibited lower circulating osteocalcin and P1NP at 2–3-months post-surgery, which was an expected finding that results from the relative cessation of longitudinal bone growth in adulthood [30, 31].

In our model, tibial diaphysis Ps.MS/BS was lower at 2-weeks and 1-month post-SCI, and Ps.BFR/BS was lower at 1 month. In comparison, distal femur and femoral diaphysis Ct.Ar and Ct.Th were lower beginning 1–2 months post-SCI. These findings suggest that a time-dependent periosteal bone formation defect occurred in response to SCI. In support of this contention, a main effect was present indicating SCI exhibited lower distal femur Tt.Ar than SHAM, suggesting impaired periosteal expansion at this skeletal site, similar to other reports [14]. In addition, our animals exhibited lower distal femur maximal load and energy to fracture beginning 2-weeks post-SCI, preceding the cortical bone structural deficits. Furthermore, distal femur BV/TV was lower, and Tb.Pf was higher 2-weeks post-SCI,

indicative of less cancellous bone and a relatively weaker and less-connected trabecular network [32]. Taken together, the early cancellous bone loss appeared to influence the impaired distal femur whole bone mechanical characteristics. Despite this, a time main effect indicated that distal femur bone strength measures improved as animals aged, which is likely explained by higher distal femur Tt.Ar in response to the renormalization of periosteal bone formation at 2 and 3 months. In comparison, femoral diaphysis bone strength measures were lower only at 2–3 months after SCI, temporally accompanying cortical bone deficits and lower TMD at this site, providing evidence that cortical bone mass also influenced bone fragility after SCI.

In addition to skeletal outcomes, we measured concentrations of select hormones that influence bone maintenance to discern the systemic effects of SCI. It is known that men with SCI often exhibit secondary hypogonadism (low testosterone) [33]. Similarly, our SCI rats exhibited 35–50% lower testosterone versus SHAM, which is roughly comparable to the magnitude of testosterone deficit in the SCI population [34]. Interestingly, the testosterone deficit in our model persisted throughout the duration of cancellous and cortical bone loss, supporting the contention that low testosterone may exacerbate bone loss after SCI [35]. In our previous studies, testosterone treatment dose-dependently prevented cancellous bone loss after SCI, with low-dose (replacement) testosterone preventing ~ 80% of cancellous bone loss and high-dose (supraphysiologic) testosterone completely preventing cancellous bone deficits [21]. We also observed persistently lower leptin in SCI versus SHAM animals that likely resulted from the initial 8–11% bodyweight loss after SCI. Interestingly, Park et al. recently reported that both fat mass and lean mass were positively associated with circulating leptin in a cohort of persons with SCI, and postulated that muscle loss leads to impaired leptin production [36]. In this regard, we have previously reported that sublesional muscle mass and muscle fiber cross-sectional area are 20–40% lower within several weeks of SCI [37], while relatively smaller differences in retroperitoneal fat mass were present among SCI and SHAM animals [21]. Regardless, it remains unknown whether an initial reduction in circulating leptin exists in persons with bodyweight loss after SCI or whether leptin influences bone homeostasis in this population. We believe these possibilities deserve consideration because (1) ~ 50% of individuals with SCI are reported to exhibit involuntary/unintended weight loss within 1 year of injury [38], (2) circulating leptin has been positively associated with BMD in wheelchair-bound men [39] and women with SCI [40], and (3) leptin treatment stimulates osteoblast proliferation and bone formation via central and peripheral pathways that are distinct from the regulation of energy metabolism [41] and attenuates disuse-mediated bone loss in rats with low leptin [42]. In addition, we evaluated circulating sclerostin, an osteocyte-derived negative regulator of the bone anabolic LRP5/LRP6-mediated Wnt/β–catenin signaling pathway, because LRP5 mRNA and several Wnt-signaling genes are downregulated in cultured osteoblasts obtained from SCI animals [28] and because mice with sclerostin gene deletion are resistant to cancellous bone loss after SCI [43]. However, no differences in circulating sclerostin were present among groups. Consistent with these observations, Gifre et al. reported that circulating sclerostin was similar among persons with recent motor-complete SCI and healthy age-matched controls [44]. Regardless, the ability of a pharmacologic anti-sclerostin antibody to potently stimulate bone formation [23, 45] and to reverse bone loss mass in rodent SCI models [29] provides

strong rationale to evaluate Romosozumab in the SCI population if this pharmacologic agent receives US Food and Drug Administration and/or European Medicines Agency approvals. Furthermore, SCI-induced alterations in other hormones, such as corticosterone and norepinephrine [46, 47], may influence skeletal homeostasis. A comprehensive analysis of all such hormones was beyond our scope, but would likely assist in elucidating factors that influence bone loss after SCI.

We were aware of previous reports delineating the early [10–12, 17] and more chronic skeletal adaptations to experimental SCI as we developed our model [8, 13–15]. However, several differences exist between these models and our 4-months-old male moderate–severe contusion SCI model. First, most previous reports assessed bone parameters in SCI and nonsurgical controls [10, 12, 14, 15, 17] or utilized baseline controls for comparison [13], which do not account for the influence of surgical stress on bone loss or for skeletal changes resulting from bone modeling, respectively. To account for these factors, we used age-/sex-matched SHAMs that underwent spinal laminectomy. Second, we used the IH impactor to induce contusion SCI, while most others employed the New York University (NYU) weight-drop system to produce moderate [14] or severe contusion SCI [10–13], or performed spinal cord transection [8, 17]. In this regard, higher impact forces worsen skeletal deficits after contusion SCI [13], with the peak force from a 250- to 300-kdyne IH Impactor being roughly equivalent to the force from a mild–moderate NYU injury [15]. Nevertheless, our SCI animals exhibited persistent hindlimb disuse consistent with severe SCI, indicating that our findings remain relevant to the severe motor-incomplete and/or motor-complete SCI populations. Of note, only one of the aforementioned studies used the IH impactor to induce moderate–severe contusion SCI and did not observe any proximal tibia cancellous bone loss at 3-months post-injury [15], which directly conflicts with our current and previous studies reporting extensive cancellous [21, 23] and cortical bone deficits [22] and pronounced muscle loss [37] in response to an identical injury severity at the same spinal level. The reasons underlying these differences remain unknown, although, our skeletally mature males did not recover the ability to support the hindlimbs in stance or to perform hindlimb stepping at any point throughout our study, while the young adult (3-months-old) females used by Lin et al. regained the ability to perform occasional weight-supported plantar stepping [15]. In this regard, young female rats have higher estradiol than males [24], which may explain some of the locomotor and skeletal differences among sexes, given that physiologic estradiol treatment is neuroprotective after SCI [48] and that estradiol prevents bone loss in ovariectomized rats undergoing hindlimb suspension [49]. This is noteworthy because our SCI animals exhibited 35–50% lower testosterone and because peripheral aromatization of testosterone is the primary source of estradiol in males [50]. Alternatively, it is possible that the force delivered to the spinal cord in our current study (average 310-kdyne) was sufficient to prevent recovery of hindlimb stepping and induce skeletal decline, while the slightly lower force employed by Lin et al. (i.e., 250-kdyne) was not. However, we find this possibility unlikely because we have previously observed that 3–5-months-old male rodents display continual hindlimb dysfunction and severe bone deficits in response to 250-kdyne contusion SCI [21–23].

In summary, our rodent moderate–severe contusion SCI model exhibited rapid cancellous bone loss and marked trabecular microarchitectural deficits, along with gradual cortical bone

loss. The cancellous bone loss resulted from increased bone resorption and concomitantly reduced bone formation, consistent with uncoupled bone turnover, while reduced periosteal bone formation indices preceded cortical bone loss. Whole bone mechanical deficits also developed in a site-specific manner after SCI, with bone strength loss at the distal femur temporally accompanying cancellous bone loss and bone strength loss at the femoral diaphysis accompanying cortical bone deficits, indicating that both cancellous and cortical bone influence whole bone mechanical characteristics after SCI. In addition, testosterone and leptin were lower in our SCI model, although, the significance of these alterations in relation to bone loss requires further investigation. In conclusion, we have developed an experimental SCI model that mimics the predominant sex, age, and injury type occurring in the human SCI population and that results in limited functional recovery and pronounced sublesional bone deterioration, demonstrating the relevance of our model in relation to the severe motor-incomplete to motor-complete SCI populations.

Supplementary Material

Refer to Web version on PubMed Central for supplementary material.

Acknowledgements

This work was supported by the Office of Research and Development, Rehabilitation Research and Development (RR&D) Service, Department of Veterans Affairs (SPiRE 1I21RX001273-01 and PECASE #B9280-O) to JFY, and by resources provided by the North Florida/South Georgia Veterans Health System. The work reported herein does not represent the views of the US Department of Veterans Affairs or the US Government.

References

1. Bauman WA, Cardozo CP (2015) Osteoporosis in individuals with spinal cord injury. PMR 7(2):188–201
2. Dauty M, Perrouin Verbe B, Maugars Y, Dubois C, Mathe JF (2000) Supralesional and sublesional bone mineral density in spinal cord-injured patients. Bone 27(2):305–309 [PubMed: 10913927]
3. Eser P, Frotzler A, Zehnder Y, Wick L, Knecht H, Denoth J, Schiessl H (2004) Relationship between the duration of paralysis and bone structure: a pQCT study of spinal cord injured individuals. Bone 34(5):869–880 [PubMed: 15121019]
4. Frotzler A, Berger M, Knecht H, Eser P (2008) Bone steady-state is established at reduced bone strength after spinal cord injury: a longitudinal study using peripheral quantitative computed tomography (pQCT). Bone 43(3):549–555 [PubMed: 18567554]
5. Frisbie JH (1997) Fractures after myelopathy: the risk quantified. J Spinal Cord Med 20(1):66–69 [PubMed: 9097259]
6. Morse LR, Battaglino RA, Stolzmann KL, Hallett LD, Waddimba A, Gagnon D, Lazzari AA, Garshick E (2009) Osteoporotic fractures and hospitalization risk in chronic spinal cord injury. Osteoporos Int 20(3):385–392 [PubMed: 18581033]
7. Grassner L, Klein B, Maier D, Buhren V, Vogel M (2017) Lower extremity fractures in patients with spinal cord injury characteristics, outcome and risk factors for non-unions. J Spinal Cord Med. 10.1080/10790268.2017.1329915
8. Jiang SD, Jiang LS, Dai LY (2007) Changes in bone mass, bone structure, bone biomechanical properties, and bone metabolism after spinal cord injury: a 6-month longitudinal study in growing rats. Calcif Tissue Int 80(3):167–175 [PubMed: 17340221]
9. Sharif-Alhoseini M, Khormali M, Rezaei M et al. (2017) Animal models of spinal cord injury: a systematic review. Spinal Cord 55(8):714–721 [PubMed: 28117332]

10. Morse L, Teng YD, Pham L et al. (2008) Spinal cord injury causes rapid osteoclastic resorption and growth plate abnormalities in growing rats (SCI-induced bone loss in growing rats). Osteoporos Int 19(5):645–652 [PubMed: 17987335]
11. Morse LR, Xu Y, Solomon B, Boyle L, Yoganathan S, Stashenko P, Battaglino RA (2011) Severe spinal cord injury causes immediate multi-cellular dysfunction at the chondro-osseous junction. Transl Stroke Res 2(4):643–650 [PubMed: 22368723]
12. Yarrow JF, Ye F, Balaez A et al. (2014) Bone loss in a new rodent model combining spinal cord injury and cast immobilization. J Musculoskelet Neuronal Interact 14(3):255–266 [PubMed: 25198220]
13. Voor MJ, Brown EH, Xu Q, Waddell SW, Burden RL Jr, Burke DA, Magnuson DS (2012) Bone loss following spinal cord injury in a rat model. J Neurotrauma 29(8):1676–1682 [PubMed: 22181016]
14. Lin T, Tong W, Chandra A et al. (2015) A comprehensive study of long-term skeletal changes after spinal cord injury in adult rats. Bone Res 3:15028 [PubMed: 26528401]
15. Lin CY, Androjna C, Rozic R, Nguyen BT, Parsons B, Midura RJ, Lee YS (2018) Differential adaptations of the musculoskeletal system following spinal cord contusion and transection in rats. J Neurotrauma 35(15):1737–1744 [PubMed: 29402167]
16. Jiang SD, Jiang LS, Dai LY (2006) Spinal cord injury causes more damage to bone mass, bone structure, biomechanical properties and bone metabolism than sciatic neurectomy in young rats. Osteoporos Int 17(10):1552–1561 [PubMed: 16874443]
17. Liu D, Zhao CQ, Li H, Jiang SD, Jiang LS, Dai LY (2008) Effects of spinal cord injury and hindlimb immobilization on sublesional and supralesional bones in young growing rats. Bone 43(1):119–125 [PubMed: 18482879]
18. Jiang SD, Shen C, Jiang LS, Dai LY (2007) Differences of bone mass and bone structure in osteopenic rat models caused by spinal cord injury and ovariectomy. Osteoporos Int 18(6):743–750 [PubMed: 17216554]
19. Devivo MJ (2012) Epidemiology of traumatic spinal cord injury: trends and future implications. Spinal Cord 50(5):365–372 [PubMed: 22270188]
20. Basso DM, Beattie MS, Bresnahan JC (1996) Graded histological and locomotor outcomes after spinal cord contusion using the NYU weight-drop device versus transection. Exp Neurol 139(2):244–256 [PubMed: 8654527]
21. Yarrow JF, Conover CF, Beggs LA et al. (2014) Testosterone dose dependently prevents bone and muscle loss in rodents after spinal cord injury. J Neurotrauma 31(9):834–845 [PubMed: 24378197]
22. Yarrow JF, Phillips EG, Conover CF et al. (2017) Testosterone plus finasteride prevents bone loss without prostate growth in a rodent spinal cord injury model. J Neurotrauma 34(21):2972–2981 [PubMed: 28338402]
23. Beggs LA, Ye F, Ghosh P et al. (2015) Sclerostin inhibition prevents spinal cord injury-induced cancellous bone loss. J Bone Miner Res 30(4):681–689 [PubMed: 25359699]
24. Yarrow JF, Conover CF, Purandare AV, Bhakta AM, Zheng N, Conrad B, Altman MK, Franz SE, Wronski TJ, Borst SE (2008) Supraphysiological testosterone enanthate administration prevents bone loss and augments bone strength in gonadectomized male and female rats. Am J Physiol Endocrinol Metab 295(5):E1213–E1222 [PubMed: 18780767]
25. McCoy SC, Yarrow JF, Conover CF et al. (2012) 17beta-Hydroxyestra-4,9,11-trien-3-one (Trenbolone) preserves bone mineral density in skeletally mature orchiectomized rats without prostate enlargement. Bone 51(4):667–673 [PubMed: 22842328]
26. Carbone LD, Chin AS, Burns SP, Svircev JN, Hoenig H, Heggeness M, Bailey L, Weaver F (2014) Mortality after lower extremity fractures in men with spinal cord injury. J Bone Miner Res 29(2):432–439 [PubMed: 23873733]
27. Reiter AL, Volk A, Vollmar J, Fromm B, Gerner HJ (2007) Changes of basic bone turnover parameters in short-term and long-term patients with spinal cord injury. Eur Spine J 16(6):771–776 [PubMed: 16830131]
28. Jiang SD, Yan J, Jiang LS, Dai LY (2011) Down-regulation of the Wnt, estrogen receptor, insulin-like growth factor-I, and bone morphogenetic protein pathways in osteoblasts from rats with chronic spinal cord injury. Joint Bone Spine 78(5):488–492 [PubMed: 21273111]

29. Zhao W, Li X, Peng Y et al. (2018) Sclerostin antibody reverses the severe sublesional bone loss in rats after chronic spinal cord injury. Calcif Tissue Int. 10.1007/s00223-018-0439-8
30. Modrowski D, del Pozo E, Miravet L (1992) Dynamics of circulating osteocalcin in rats during growth and under experimental conditions. Horm Metab Res 24(10):474–477 [PubMed: 1464413]
31. Han B, Copeland M, Geiser AG, Hale LV, Harvey A, Ma YL, Powers CS, Sato M, You J, Hale JE (2007) Development of a highly sensitive, high-throughput, mass spectrometry-based assay for rat procollagen type-I N-terminal propeptide (PINP) to measure bone formation activity. J Proteome Res 6(11):4218–4229 [PubMed: 17924680]
32. Ito M, Nishida A, Koga A, Ikeda S, Shiraishi A, Uetani M, Hayashi K, Nakamura T (2002) Contribution of trabecular and cortical components to the mechanical properties of bone and their regulating parameters. Bone 31(3):351–358 [PubMed: 12231406]
33. Bauman WA, La Fountaine MF, Cirnigliaro CM, Kirshblum SC, Spungen AM (2017) Testicular responses to hCG stimulation at varying doses in men with spinal cord injury. Spinal Cord 55(7):659–663 [PubMed: 28220820]
34. Sullivan SD, Nash MS, Tefera E, Tinsley E, Blackman MR, Groah S (2017) Prevalence and etiology of hypogonadism in young men with chronic spinal cord injury: a cross-sectional analysis from two university-based rehabilitation centers. PMR 9(8):751–760
35. Maimoun L, Lumbroso S, Paris F, Couret I, Peruchon E, Rouays-Mabit E, Rossi M, Leroux JL, Sultan C (2006) The role of androgens or growth factors in the bone resorption process in recent spinal cord injured patients: a cross-sectional study. Spinal Cord 44(12):791–797 [PubMed: 16568142]
36. Park AJ, Battaglino RA, Nguyen NMH, Morse LR (2018) Associations between lean mass and leptin in men with chronic spinal cord injury: results from the FRASCI-muscle study. PLoS ONE 13(6):e0198969 [PubMed: 29949600]
37. Phillips EG, Beggs LA, Ye F, Conover CF, Beck DT, Otzel DM, Ghosh P, Bassit ACF, Borst SE, Yarrow JF (2018) Effects of pharmacologic sclerostin inhibition or testosterone administration on soleus muscle atrophy in rodents after spinal cord injury. PLoS ONE 13(3):e0194440 [PubMed: 29579075]
38. Powell D, Affuso O, Chen Y (2017) Weight change after spinal cord injury. J Spinal Cord Med 40(2):130–137 [PubMed: 25353325]
39. Doubelt I, Totosy de Zepetnek J, MacDonald MJ, Atkinson SA (2015) Influences of nutrition and adiposity on bone mineral density in individuals with chronic spinal cord injury: A cross-sectional, observational study. Bone Rep 2:26–31 [PubMed: 28377950]
40. Sabour H, Norouzi Javidan A, Latifi S, Shidfar F, Vafa MR, Emami Razavi SH, Larijani B, Heshmat R (2015) Relationship between leptin and adiponectin concentrations in plasma and femoral and spinal bone mineral density in spinal cord-injured individuals. Spine J 15(1):1–9 [PubMed: 24948038]
41. Turner RT, Kalra SP, Wong CP, Philbrick KA, Lindenmaier LB, Boghossian S, Iwaniec UT (2013) Peripheral leptin regulates bone formation. J Bone Miner Res 28(1):22–34 [PubMed: 22887758]
42. Baek K, Bloomfield SA (2009) Beta-adrenergic blockade and leptin replacement effectively mitigate disuse bone loss. J Bone Miner Res 24(5):792–799 [PubMed: 19113907]
43. Qin W, Li X, Peng Y et al. (2016) Sclerostin antibody preserves the morphology and structure of osteocytes and blocks the severe skeletal deterioration after motor-complete spinal cord injury in rats. J Bone Miner Res 31(7):1482 [PubMed: 27377772]
44. Gifre L, Vidal J, Carrasco JL, Filella X, Ruiz-Gaspa S, Muxi A, Portell E, Monegal A, Guanabens N, Peris P (2015) Effect of recent spinal cord injury on wnt signaling antagonists (sclerostin and dkk-1) and their relationship with bone loss. A 12-month prospective study. J Bone Miner Res 30(6):1014–1021 [PubMed: 25484108]
45. Qin W, Li X, Peng Y et al. (2015) Sclerostin antibody preserves the morphology and structure of osteocytes and blocks the severe skeletal deterioration after motor-complete spinal cord injury in rats. J Bone Miner Res 30(11):1994–2004 [PubMed: 25974843]
46. Pruss H, Tedeschi A, Thiriot A et al. (2017) Spinal cord injury-induced immunodeficiency is mediated by a sympathetic-neuroendocrine adrenal reflex. Nat Neurosci 20(11):1549–1559 [PubMed: 28920935]

47. Zhang Y, Guan Z, Reader B et al. (2013) Autonomic dysreflexia causes chronic immune suppression after spinal cord injury. J Neurosci 33(32):12970–12981 [PubMed: 23926252]

48. Samantaray S, Das A, Matzelle DC, Yu SP, Wei L, Varma A, Ray SK, Banik NL (2016) Administration of low dose estrogen attenuates persistent inflammation, promotes angiogenesis, and improves locomotor function following chronic spinal cord injury in rats. J Neurochem 137(4):604–617 [PubMed: 26998684]

49. Yarrow JF, McCoy SC, Ferreira JA, Pingel JE, Conrad BP, Wronski TJ, Williams AA, Borst SE, Brown M (2012) A rehabilitation exercise program induces severe bone mineral deficits in estrogen-deficient rats after extended disuse. Menopause 19(11):1267–1276 [PubMed: 22713863]

50. Yarrow JF, Wronski TJ, Borst SE (2015) Testosterone and adult male bone: actions independent of 5 alpha-reductase and aromatase. Exerc Sport Sci Rev 43(4):222–230 [PubMed: 26196865]

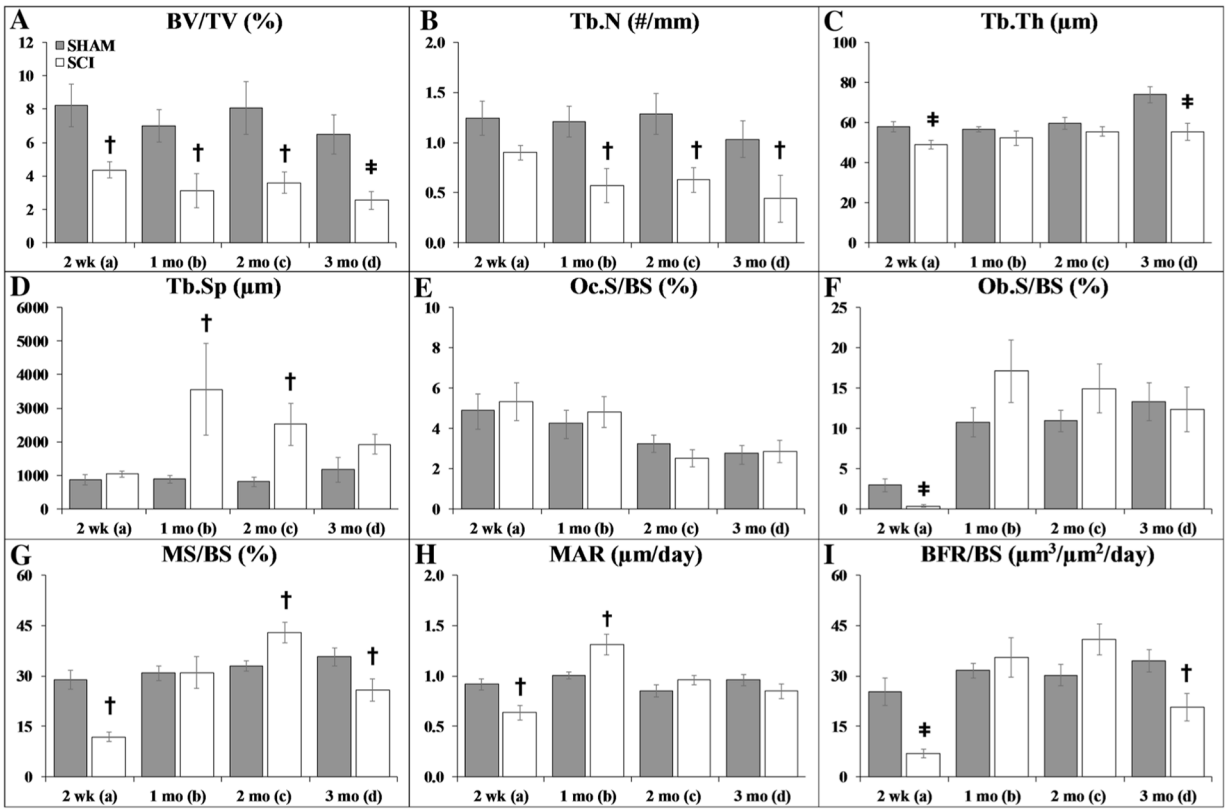

Fig. 1.

a–**i** Cancellous histomorphometric outcomes at the proximal tibial metaphysis. Values are means ± SEM, n = 8–15/group at each timepoint. Dagger indicates $p < 0.05$ and ǂ indicates $p < 0.01$ for SHAM versus SCI at the same time point derived from t-tests. Main effects and interactions derived from the 2 × 4 ANOVAs are reported in Online Resource 4

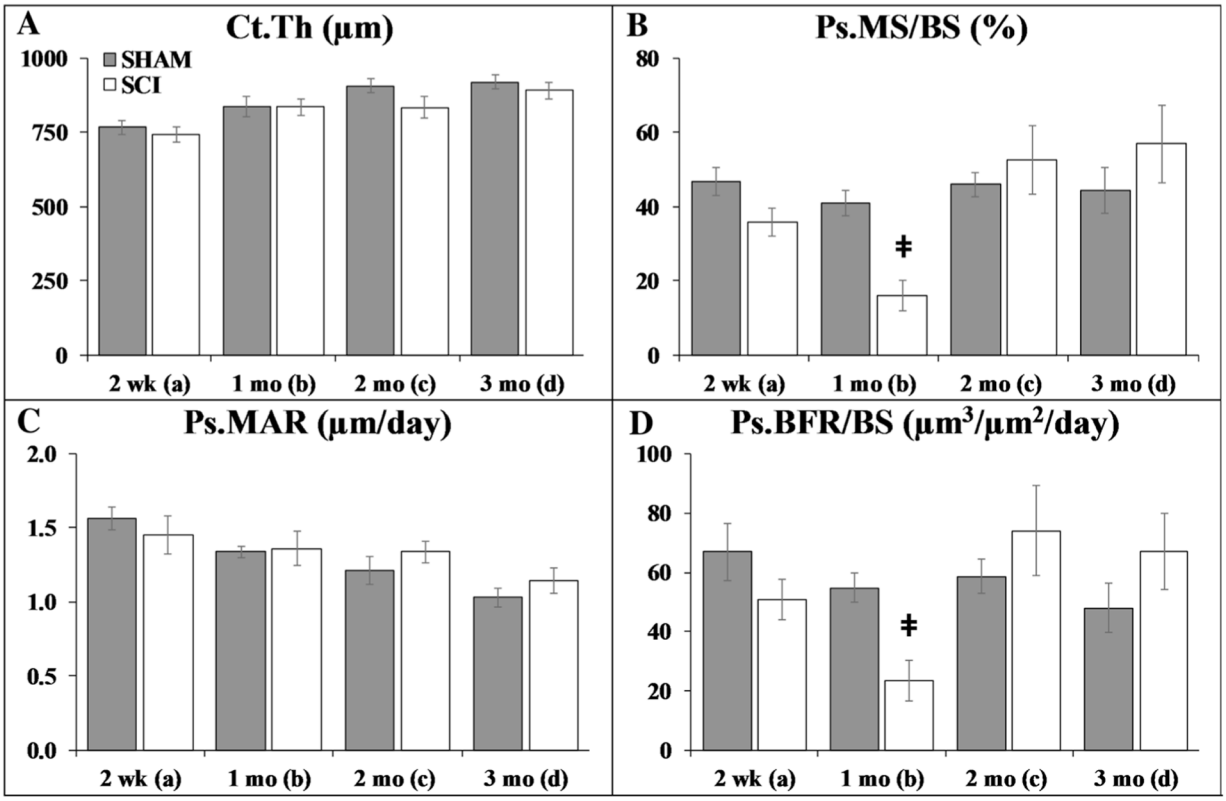

Fig. 2.

a–**d** Cortical histomorphometric outcomes at the tibial diaphysis. Values are means ± SEM, n = 8–14/group at each timepoint. Dagger indicates $p < 0.05$ and ‡ indicates $p < 0.01$ for SHAM versus SCI at the same timepoint derived from t-tests. No endocortical differences were present among groups, and no double-fluorochrome labeling was present for Ec.MAR or Ec.BFR/BS (not shown). Main effects and interactions derived from the 2 × 4 ANOVAs are reported in Online Resource 4

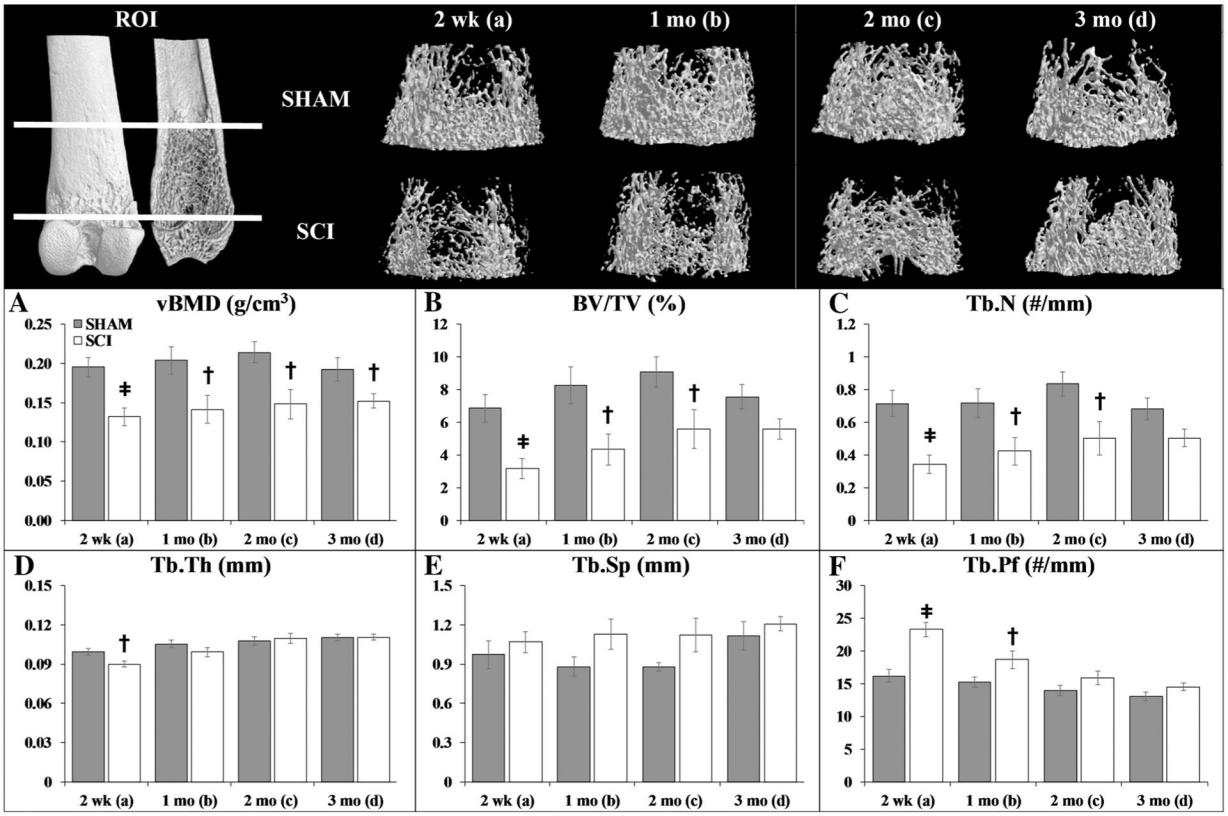

Fig. 3.

a–f Representative microcomputed tomography (μCT)-based cancellous bone images and morphologic outcomes at the distal femoral metaphysis region of interest (ROI). Values are means ± SEM, $n = 9–17$/group at each timepoint. Dagger indicates $p < 0.05$ and ǂ indicates $p < 0.01$ for SHAM versus SCI at the same timepoint derived from *t*-tests. Main effects and interactions derived from the 2 × 4 ANOVAs are reported in Online Resource 4

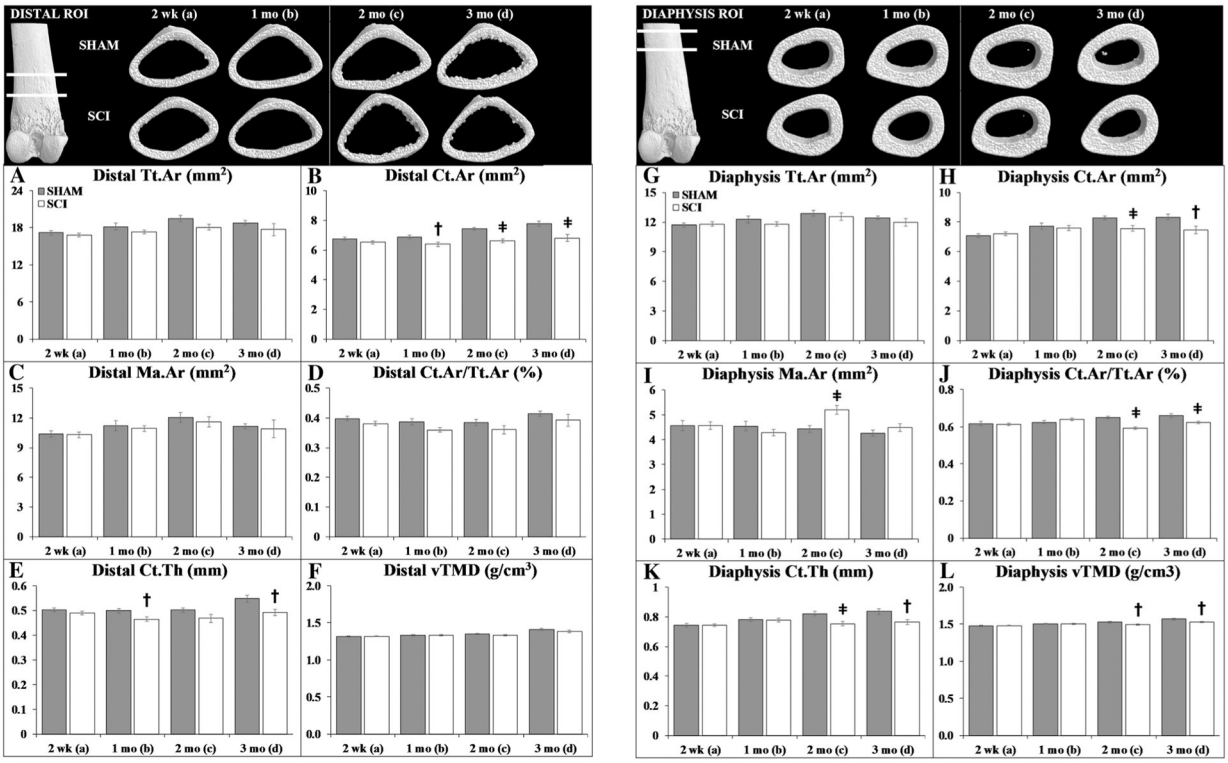

Fig. 4.

a–l Representative microcomputed tomography (μCT)-based cortical bone images and morphologic outcomes at the distal femur and femoral diaphysis region of interest (ROI). Values are means ± SEM, $n = 9–17$/group at each timepoint. Dagger indicates $p < 0.05$ and ǂ indicates $p < 0.01$ for SHAM versus SCI at the same timepoint derived from *t*-tests. Main effects and interactions derived from the 2 × 4 ANOVAs are reported in Online Resource 4

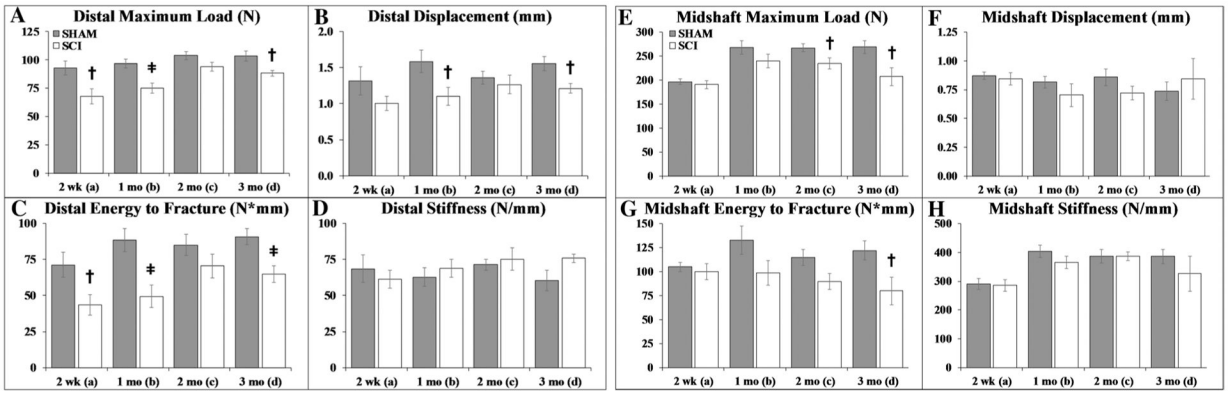

Fig. 5.

a–**h** Distal femur and femoral midshaft bone mechanical characteristics. Values are means ± SEM, $n = 7–10$ per group at each timepoint. Dagger indicates $p < 0.05$ and ǂ indicates $p < 0.01$ for SHAM versus SCI at the same timepoint derived from *t*-tests. Main effects and interactions derived from the 2 × 4 ANOVAs are reported in Online Resource 4

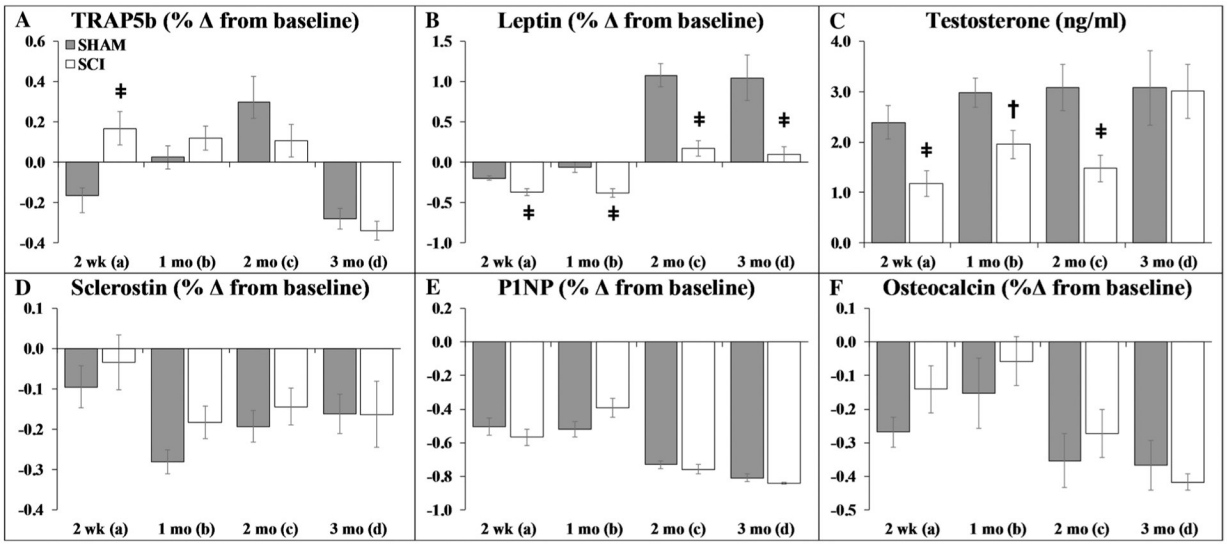

Fig. 6.

a–**f** Circulating hormone responses. Values are means ± SEM of the percentage change from baseline, except for testosterone which is the actual concentration (due to insufficient sera to determine baseline values on all samples), n = 10–30/group at each timepoint. Dagger indicates $p < 0.05$ and ǂ indicates $p < 0.01$ for SHAM versus SCI at the same timepoint derived from t-tests. Main effects and interactions derived from the 2 × 4 ANOVAs are reported in Online Resource 4